Determine the Orientation of β-Sheet Conformation for Specific Residues in N-Terminus of α-syn(61－95) in Monolayer by pMAIRS

By

Olatayo Adedayo Olahanmi

A Thesis Submitted in Partial Fulfillment of the Requirements for the Degree of Master of Science in Chemistry

Middle Tennessee State University
December 2024

Thesis Committee:

Dr. Chengshan Wang. Chair

Dr. Jing Kong

Dr. Ngee Chong

Special appreciation to my Parents, Prince & Mrs. S.A Olahanmi, my siblings, and my dearest Oluwatunmise.

ABSTRACT

Parkinson's disease (PD) is the second most common neurodegenerative disorder, and the hallmark of PD is the presence of Lewy bodies in the midbrain. The protein component of Lewy bodies is α-synuclein, a protein that consists of 140 amino acids. The sequence of α-synuclein can be divided into three distinct domains, namely, the N-terminus domain, the non-amyloid component domain or NAC, and the C-terminus domain. The NAC domain consisting of residues 61-95 has been of utmost importance due to the disordered self-assembly behavior. In addition, NAC and other segment peptides have been detected in Lewy bodies. Previously in our research group, NAC was investigated by p-Polarized Multiple Angle Incidence Resolution Spectroscopy (pMAIRS) which can be used to detect the orientation of various vibrations in ultrathin films (such as monolayer). The overall conformation of NAC in a freshly prepared monolayer structure was shown to be α-helix. In addition, ^{13}C isotopic label has been introduced into residue 93C in NAC. By pMAIRS, the orientation of α-helix at 93G is parallel to the interface. In this thesis, the monolayer of NAC was compressed for several days, and β-sheet conformation was detected in the monolayer of NAC. By introducing ^{13}C isotopic label into the other residues in the sequence of NAC, 93G was found to be still in α-helix after three days compression. However, the N-terminus residue (68G) changed its conformation from α-helix to β-sheet after three days compression. Moreover, 63V which is closer to the N-terminus changed its conformation after only two days compression. Furthermore, edge-up orientation was detected for the newly generated β-sheet conformation. Therefore, the capability of pMAIRS to analyze the structure of membrane proteins in a monolayer with residue-level resolution was demonstrated.

ACKNOWLEDGEMENTS

My sincere gratitude goes out to Dr. Chengshan Wang, my research adviser, for his tremendous advice and unwavering support during the course of my thesis research. My success has been greatly attributed to his readiness to listen and put my needs first.

Additionally, I would like to thank Dr. Jing Kong and Dr. Ngee Chong from my thesis committee for their time spent examining my thesis and offering insightful criticism of my work.

I would especially like to express my gratitude to the MTSU College of Graduate Studies and the College of Basic and Applied Sciences for supporting and providing programs that allow students such as myself to share and present our research. The chemistry department at MTSU has been a great help in advancing my professional objectives by offering tools to support my chemical research.

Also, I want to thank Jessie Weatherly for his assistance with troubleshooting and fixing the instrument when we had a breakdown. I would thank Dami and Toyin who are members of Dr Wang's lab for their teamwork efforts, time, and sacrifices towards the success of the group.

TABLE OF CONTENTS

LIST OF FIGURES

LIST OF TABLES

CHAPTER 1

INTRODUCTION

1.1 Protein and Membrane Protein.

Determining the structure of proteins is a crucial topic in biochemistry as they facilitate and carry out the biochemical processes that occur in vivo.[1-3] Amino acids are the building blocks of protein, and there are twenty different amino acids in nature.[1-3] The amine and carboxylic groups present in all amino acids are linked by α-carbon to the R group, which distinguishes them from one another. Amino acids can be covalently bonded to form proteins by forming an amide bond between the carboxylic group and the adjacent amine group. The primary structure is the sequence of amino acids in a protein. Proteins can then fold to create various secondary structures, also known as conformations, such as α-helix, β-sheet, random coils, and so on.[1-3] Of all proteins, membrane proteins are involved in both endogenous and exogenous processes, and their malfunction can result in a variety of diseases.[4-8] For example, α-synuclein (α-syn) is a membrane protein, and its abnormal aggregation has been reported to cause Parkinson's disease.

1.2 α-Synuclein (α-syn) and α-Syn(61－95) Segment.

α-syn is a 140-amino-acid protein (sequence shown in Figure 1-1 below)[9, 10] which accumulates in presynaptic terminals where vesicles and other membrane structures are predominantly present.[11, 12] Although the function is still not known, α-syn is the major protein component in Lewy bodies which are the abnormal hallmark aggregates in the brain of Parkinson's disease (PD) patients.[9,10] It is important to note that Lewy bodies also contain α-syn

segment peptides. Three regions have been identified in the α-syn sequence: the C-terminus (residues 96-140), non-amyloid component (residues (61－95), and N-terminus (residues 1-60). [13] Although the name α-syn(61－95) refers to a non-amyloid component, it is highly prone to aggregation and has been found in Lewy bodies alongside the α-syn whole protein. [14] Alzheimer's disease (AD) patients' brains have been shown to contain β-amyloid peptide and α-syn(61－95) in senile plaques. [15]

MDVFMKGLSK AKEGVVAAAE KTKQGVAEAA GKTKEGVLYV GSKTKEGVVH GVATVAEKTK EQVTNVGGAV VTGVTAVAQK TVEGAGSIAA ATGFVKKDQL GKNEEGAPQE GILEDMPVDP DNEAYEMPSE EGYQDYEPEA

Figure 1-1. The sequence of α-syn with the N-terminus in Italics and the NAC region is underlined.

Despite its considerable relevance with AD and PD, the biophysical and biochemical investigation of α-syn(61－95) has long been ignored. The structure information for α-syn entire protein and α-syn(61－95) is restricted due to membrane protein problems for significant approaches to address protein structure.

1.3 Challenges of Membrane Proteins in Structural Determination.

The three-dimensional (3D) structures of proteins and peptides can be determined with atomic resolution by X-ray crystallography, which is a popular method.[3, 16, 17] Nevertheless, this method

is restricted by problems of crystallization of many integral membrane proteins with the feature that single crystals are extremely difficult to obtain for analysis. As a very useful technique, Nuclear Magnetic Resonance (NMR) spectroscopy also has obstacles to being applied to membrane-associated proteins because the repetitive sequences in roles bring about severe signal overlap, making it hard to acquire accurate results.[6] Furthermore, cell membranes are composed of phospholipid bilayers, and the inclusion of membrane proteins in the fluid matrix slows down their rate of tumbling, making it difficult to interpret structural information from NMR.[6] On the other hand, cryo-electron microscopy (cryo-EM) has made remarkable progress in recent years as a high-resolution method for more accurately defining membrane protein and peptide structures.[4, 7] Cryo-EM samples are typically applied to cryo-grids, which consist of a metal support grid atop a holey carbon film for better distribution and alignment of proteins/peptides.[18] At the same time, it is not surprising that cryo-EM strongly encourages strip proteins to already have two conformations co-existing with each other (or stationing at an equilibrium position) before they can carry out a conformational change.[19]

It is important to note that vesicles and cell membranes are typically surrounded by a monolayer structure made of membrane protein.[19,20] Membrane proteins either form transmembrane structures or lie parallel to the membrane's surface in a monolayer.[19, 20] Note that all three main approaches are reserved for large protein samples. In other words, none of them can provide high-resolution results for proteins in monolayer structure, which is the native state of membrane proteins. Therefore, surface techniques have been developed to address this issue. For example, the morphology of monolayers has been studied using Atomic Force Microscopy (AFM), and their thickness has been assessed using ellipsometry and small-angle X-ray

diffraction.[21,22] In addition, as membrane proteins exhibit a similar amphiphilic nature to cell membranes, the structure of membrane proteins in monolayers can be studied by combining surface spectroscopic techniques with the air-water interface.[23, 24] Among various techniques, FTIR is an important one as described below.

1.4 FTIR Spectroscopy for Proteins and Surface on Monolayer Analysis.

FTIR spectroscopy is another useful method to evaluate peptide/protein's major secondary structure.[25] The amide I band's distinctive peak position, which ranges (from 1600 to 1700 cm^{-1}), primarily results from the stretching mode vibration of the backbone carbonyls (i.e., C=O). For example, the amide I band of α-helix is around 1650 cm^{-1}, whereas that of β-sheet is at 1630 cm^{-1}, and that of the unstructured conformation is at 1640 cm^{-1}.[25] By deconvoluting the amide I band, the major conformation in a peptide/protein can be evaluated.[12, 25] Together with a supported phospholipids bilayer (SPB) structure mimicking cell membrane,[20, 26] Surface FTIR techniques have been used to evaluate the orientation of membrane peptides/proteins at the interface.[25, 27, 28] The major surface FTIR techniques, namely, Infrared External Reflection Spectroscopy (IR-ERS), Attenuated Total Reflection (ATR), and p-polarized Multiple Angle Incidence Resolution Spectroscopy (pMAIRS).

In contrast to early surface FT-IR techniques like the ATR technique and IR-ERS, pMAIRS demonstrates a novel advantage.[22] For example, ATR can only be applied to a limited number of substrates with high refractive index, but pMAIRS can be applied to a much wider range of substrates (e.g., CaF_2).[22] As for IR-ERS, the orientation of transition moments is ascertained by reflecting light from an irradiated p-polarized infrared beam. The p-polarized infrared beam's

reflection around the magic angle (i.e., 53.5) is nearly zero, making it challenging for IR-ERS to perform a quantitative assessment regarding the tilted angle of transition moments surrounding the magic angle.[22] In addition, theoretical calculations and experimental measurements are needed for IR-ERS to perform a quantitative evolution of the tilted angle of a transition moment. Many researchers find it challenging to use IR-ERS because of the requirements mentioned earlier.[22] In contrast, the measurements of pMAIRS are straight forward and the results are decomposed to in-plane (IP) spectrum and out-of-plane (IP) spectrum automatically after the measurement. The IP results contain all the transition moments parallel to the surface of the substrate, and the OP contains the perpendicular ones. The tilted angle 90-ϕ of a transition moment can be quantitatively evaluated by Equation 1 below. A_{IP} and A_{OP} are the peak intensity of a vibration in IP and OP results, respectively.[29, 30] The tilted angle/orientation of various conformations or secondary structures in a peptide/protein can also be accurately determined as shown below in Figure 1-2.

$$\phi = \tan^{-1}\sqrt{\frac{2A_{IP}}{A_{OP}}} \qquad \text{Equation (1)}$$

As illustrated in Figure 1-2A, the α-helix stretching mode vibration of the backbone C=O is approximately parallel to the α-helix axis direction.[31] Therefore, the amide I band in pMAIRS can be used to determine the orientation of the α-helix axis. Regarding the strand in β-sheet conformation, Figure 1-2B illustrates that its orientation is perpendicular to both the C=O backbone and the C_α–H. Thus, the amide I band and the C_α–H in pMAIRS can also precisely determine the orientation of the strand in β-sheet conformation.[32] For example, both the backbone C=O and C_α–H will be parallel to the surface of SPB if the strand in β-sheet

conformation is perpendicular to the surface, as shown in Figure 1-2B.[32] Thus, our group started to study the surface chemistry of α-syn(61－95) by air-water interface,[23, 24, 29, 30, 33] which shows similar properties to the amphiphilic natures (such as vesicles and cell membranes) with high concentration existing in the presynaptic terminals.[13, 34] α-Syn(61－95) was found to form a monolayer at the air-water interface and be unstructured in aqueous solution.[29] More importantly, α-syn(61－95) in monolayer structure was also examined using surface FT-IR as shown below.

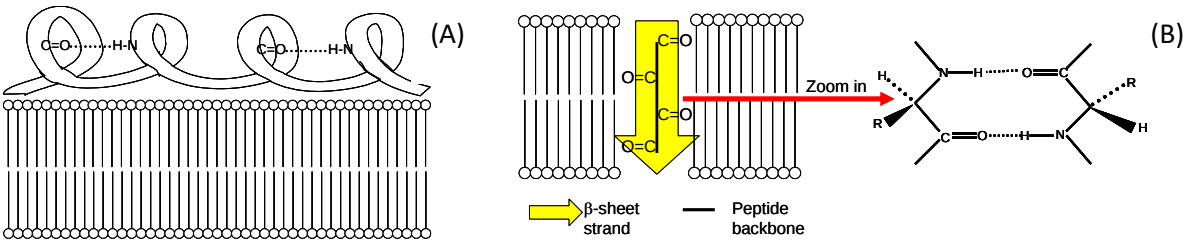

Figure 1-2. The illustration about the orientation of (A) α-helix on supported phospholipid bilayer (SPB) and (B) β-sheet strand perpendicular to the SPB (middle) and the enlargement of a typical residue with both the C=O and C_{α}–H parallel to the surface of SPB (right).

1.5 Surface Chemistry and Spectroscopy of α-Syn(61-95) at Air-Water Interface.

The surface pressure-area (π－A) isotherm of α-Syn(61－95) is depicted in Figure 1-3. The (π－A) isotherm's lift-off point for pure water subphase was 400 $Å^2$/molecule. Subsequently, the surface pressure increased steadily until it reached a kink point at 360 $Å^2$/molecule. The surface pressure rapidly increased when the surface area was further reduced, and the collapse was noticed at 205 $Å^2$/molecule with a surface pressure of 17 mN/m. The isotherm's higher surface

pressures were extrapolated to a nil surface pressure, yielding the limiting molecular area of 350 $Å^2$/molecule. When a high concentration of NaCl (0.5 M) was added into the subphase, the limiting molecular area did not increase much (cf, the dashed line in Figure 1-3). This means that the amphiphilic nature of the interface is the major reason to keep α-syn(61－95) at the interface.

Subsequently, an intriguing question emerges: why is α-syn(61－95) maintained at the interface? This is because α-syn(61－95) is an unstructured conformation in aqueous solution, and it does not exhibit a preference to remain at the interface. In order to investigate this matter, a Langmuir monolayer of α-syn(61－95) was placed onto quartz slides in the form of a Langmuir-Blodgett (LB) film. Figure 1-4 displays the CD spectra of the LB film as well as the aqueous solution of α-syn(61－95).

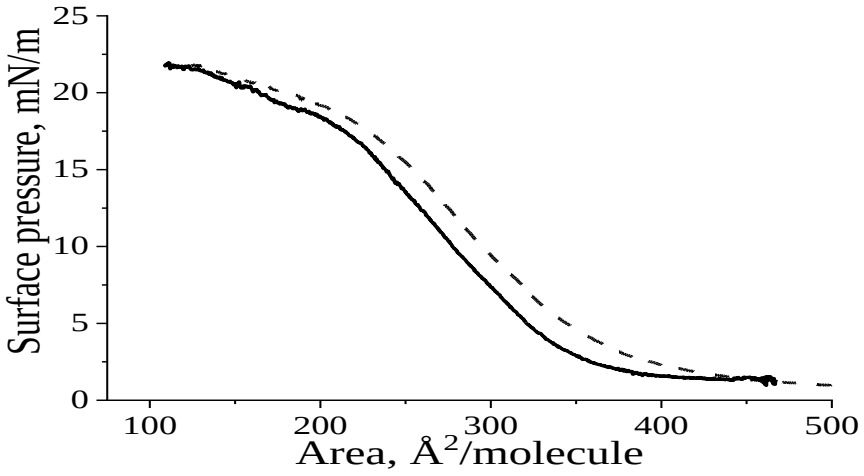

Figure 1-3 Surface pressure-area isotherm of α-syn(61－95) on: pure water (solid line) and 0.5 M NaCl (dashed line). Adapted from reference with permission[29].

There is just one negative peak at 199 nm for the α-syn(61－95) in aqueous solution, and it is attributed to an unstructured conformation.[33] An additional positive peak at 191 nm was found along with two negative peaks at 208 & 221 nm in the LB film of α-syn(61－95) on quartz slides.[33] Since all of the peaks above are α-helix characteristics, α-syn(61－95) changes into an α-helix in the LB film. The Langmuir monolayer of α-syn(61－95) was transferred onto a silicon substrate under 6 mN/m and analyzed by pMAIRS in order to ensure the α-helical conformation of the α-syn(61－95) at the interface and ascertain the tilt angle of the axis of an α-helix to the interface.

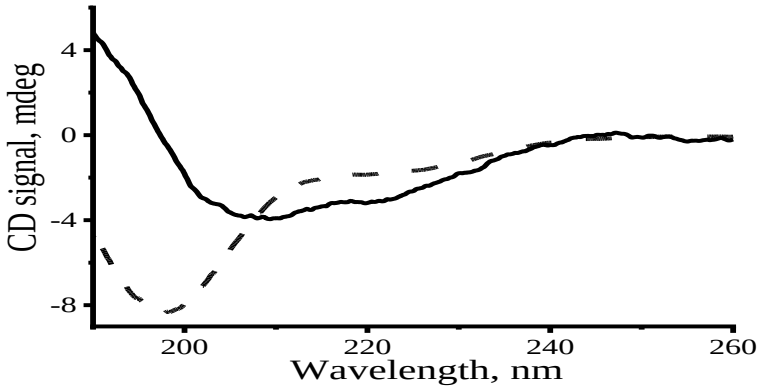

Figure 1-4. Circular Dichroism spectra of α-syn Langmuir-Blodgett film on quartz slides (solid line curve) under 6 mN/m and 0.075 mg/mL α-syn(61－95) dissolved in pure water (dashed line curve), respectively. Adapted from reference with permission[29-30].

Figure 1-5 shows that the amide I band at 1658 cm^{-1}, the characteristic peak of α-helix, was detected in both the S_{IP} and S_{OP} in the pMAIRS spectra of α-syn(61－95)[29] It was discovered

that at the interface, α-syn(61－95) transformed into an α-helix in conjunction with Circular Dichroism (CD) spectroscopy. In addition, the tilted angle of the axis of α-helical α-syn(61-95) was examined by p-polarized Multiple-Angle Incidence Resolution Spectrometry (pMAIRS) by Equation 1 mentioned above.[29, 30] Roughly, the peak intensity of the amide I band at 1658 cm^{-1} in S_{IP} and S_{OP} in Figure 1-5 is used to evaluate the tilt angle of the amide I transition moment to be 30.1º.

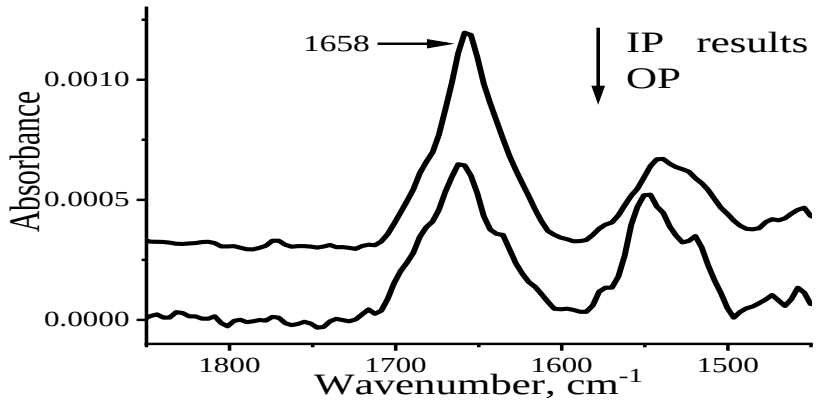

Figure 1-5. p-MAIRS results of the LB film of α-syn(61－95) transferred under 6 mN/m. Adapted from reference with permission[29].

1.6 ^{13}C Isotope Edited FTIR and pMAIRS.

It is worth noting that the traditional FT-IR technique can only provide “low-resolution” results, which cannot be used to address a specific residue's conformation or orientation.[31] For instance, a membrane protein with a 0º tilt angle lies parallel the membrane, whereas a protein with a 90º tilt angle forms a transmembrane structure. Therefore, there are two likely answers to the question, as shown in Figure 1-6, regarding the behavior of α-syn(61－95) at the interface: will it form a

transmembrane structure or be parallel to the interface, given 30.1º, which is the average tilt angle of the axis at all thirty-five residues in α-syn(61－95). One possibility is that the axis of all the thirty-five amino acid residues is 30.1º, as shown in Figure 1-6A. The other is that the axis of some residues is parallel, whereas that of other residues is perpendicular, as illustrated in Figure 1-6B. The overall tilt angle of Figure 1-6B is also around 30.1 º. To address this issue, technique with a higher resolution (such as residue level resolution) result is needed.

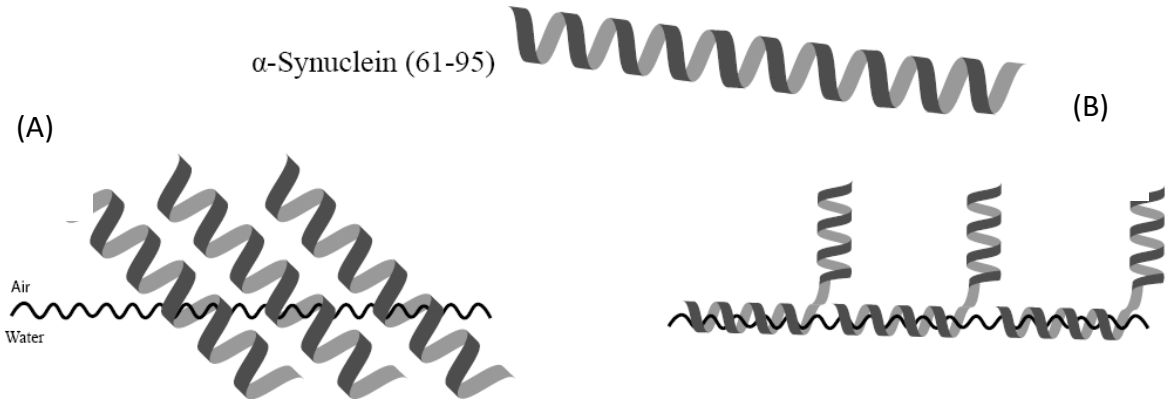

Figure 1-6. Illustration of two probabilities of α-syn(61－95) at the air-water interface. Adapted from reference with permission[30].

Recently, the ^{13}C isotope-edited FT-IR spectroscopy was developed to provide residue level resolution by introducing ^{13}C isotopic labels into the backbone carbonyl (i.e., C=O) of a peptide/protein.[31, 35] The ^{13}C labeled C=O will generate a ^{13}C amide I band which can provide the conformation of a specific residue.[31, 36, 37] It has been noted that the biophysical behavior (such as conformation and orientation) of residues near the end of a sequence may differ from that of residues in the middle.[37] Our research group placed ^{13}C isotopic label into the sequence of α-

syn(61-95) in the backbone C=O of the glycine at position 93 (i.e., 93G), which is close to the C-terminus. This serves as a proof-of-principle example. Figure 1-7 displays the pMAIRS results for ^{13}C -labeled α-syn(61-95) at 93G. Figure 1-7 shows the in-plane spectrum S_{IP} of ^{13}C labeled α-syn(61-95). Similar to previously described unlabeled α-syn(61-95), [29] regular amide I and II bands of the α-helix were identified at 1655 and 1535 cm^{-1}, respectively. However, a very strong ^{13}C amide I band was found at 1625 cm^{-1} in the IP spectrum shown in Figure 1-7. The peak at 1625 cm^{-1} cannot be assigned to the β-sheets conformation because no signal of β-sheets was detected in the CD result. In addition, the ^{13}C amide I band in the IP spectrum is more intensive than the regular amide I band at 1655 cm^{-1}, which is the sum absorption of all the other thirty-four residues in the sequence of α-syn(61－95).As described in the selection rule in previous publication,[22] the peak intensity in pMAIRS can be affected by several factors such as thickness of the sample and the orientation of the transition moment. In the monolayer, the thickness of all the residues are almost the same and the orientation is the major factor to affect the peak intensity. Therefore, such an intensive ^{13}C amide I band suggests a very small tilt angle (i.e., parallel orientation) of the ^{13}C amide I transition moment.

The out-of-plane spectrum (S_{OP}) which is the bottom curve in Figure 1-7 correlates to the IP spectrum and confirms this conclusion. The regular amide I and II bands were also detected in the S_{OP}. The regular amide I band splits slightly to 1659 and 1645 cm^{-1}, possibly stemming from the coupling between the regular and the ^{13}C amide I transition moment.[6] More importantly, the ^{13}C amide I band at 1625 cm^{-1} was very weak in the S_{OP} (i.e., the A_{OP} is almost zero for Equation 1 shown above), even though the ^{13}C label does exist at position 93G. According to the selection rule of pMAIRS shown in Equation 1 above, the tilt angle of the ^{13}C amide I transition moment at

93G is ~0º because the A_{OP} is almost zero. Consequently, the case shown in Figure 1-6B is the truth by the ^{13}C edited pMAIRS.

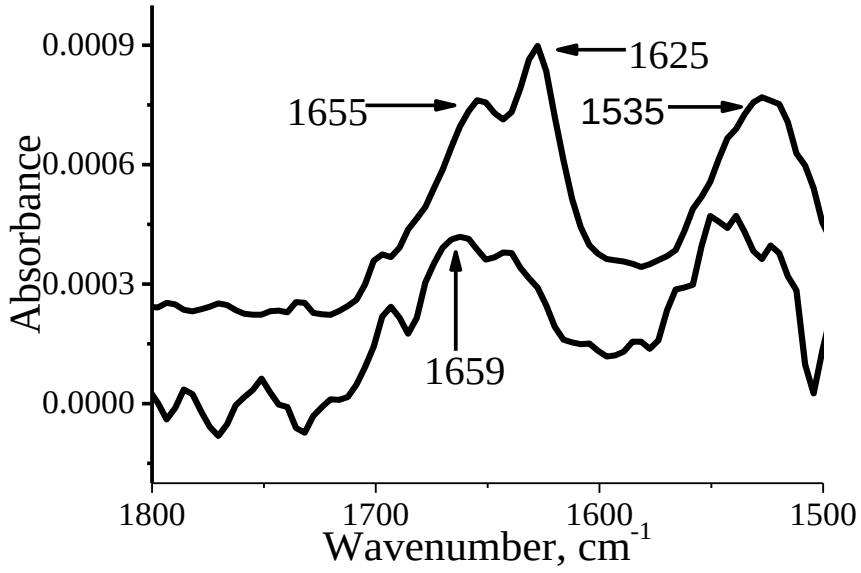

Figure 1-7. pMAIRS results of the LB monolayer of the ^{13}C labeled α-syn(61－95)) at position 93G prepared at 10 mN/m on silicon slide. The top curve is the IP spectrum, and the bottom one is OP spectrum. Adapted from reference with permission[30].

1.7 Conformation Change of α-Syn(61－95) with Long Time Compression.

The stability study of Langmuir monolayer of α-syn(61－95) is shown in Figure 1.8. Over the course of two hours, the surface pressure of α-syn(61－95) Langmuir monolayer was maintained at 6mN/m through compression. Throughout the whole experiment, the surface pressure (solid line curve) and area (dashed line curve) were recorded (*c.f.*, Figure 1-8). Similar to what is seen in Figure 1-3, the area decreased as the surface pressure rose from 0 to 6 mN/m.[29]

After reaching 6 mN/m, the molecular area decreased more than 30 % within the first one hour. After that, the molecular area decreased only about 1% for the second hour compression. As discussed above,[29] α-syn(61－95) transformed to α-helix at the interface shortly (roughly after 15 minutes compression) after it was spread there by studying α-syn(61－95) monolayer by various spectroscopic techniques. Then, what happened during the two hours compression which caused the significant decreasing of the molecular area? As reported, α-syn is unstructured in aqueous solution and transforms to α-helix in the presence of membrane. More importantly, α-syn aggregates to β-sheet conformation in Lewy Bodies. Is there any conformation change of α-syn(61－95) during the compression? To address the significant questions above, ^{13}C label was also introduced to the backbone carbonyl of 68G in the N-terminus of α-syn(61－95). The ^{13}C labeled sample was also spread at the interface to form monolayer, which was then studied by pMAIRS as below.

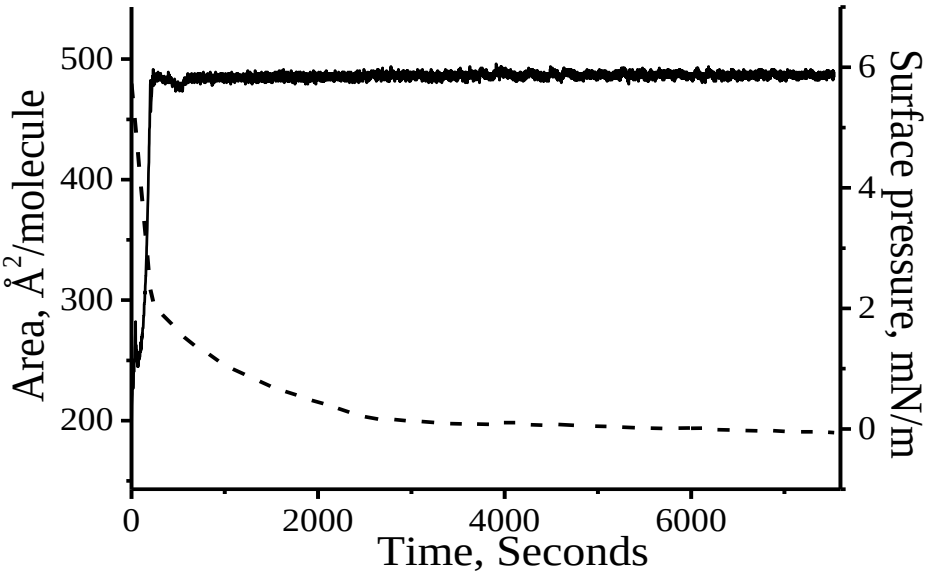

Figure 1-8. Stability curves when the Langmuir monolayer of α-syn(61－95) was compressed up to 6mN/m and kept constant for more than two hours on pure water subphase. Solid curve is for surface pressure and dashed curve is for molecular area. Adapted from reference with permission[30].

Figure 1-9 depicts the pMAIRS result containing S_{IP} and S_{OP} of the monolayer of unlabeled α-syn(61－95) transferred after two hours compression at 6 mN/m. As mentioned above, the pMAIRS results of the monolayer of unlabeled α-syn(61－95) transferred after compression at 6 mN/m for 15 minutes have been shown in Figure 1-5.[29] Similar to the Figure 1-5, the peak position of amide I band in both IP and OP spectra is at 1658 cm^{-1} which is the characteristic peak of α-helix. Therefore, α-helix is still the major conformation of α-syn(61－95) during the two hours compression. However, the intensity of the peak at 1658 cm^{-1} in S_{OP} result was lower than that transferred at 6 mN/m for 15 minutes as shown in Figure 1-5.[29] After calculation by the peak intensity at 1658 cm^{-1} according to Equation 1, the tilt angle of the amide I transition moment after two hours compression is 21.2º, also significantly lower than ~30.1 º calculated from Figure 1-5.[29] This difference in the tilt angle indicates that the surface area in Figure 1-8 is rapidly decreasing because the amide I transition moment of the α-helix becomes more parallel.

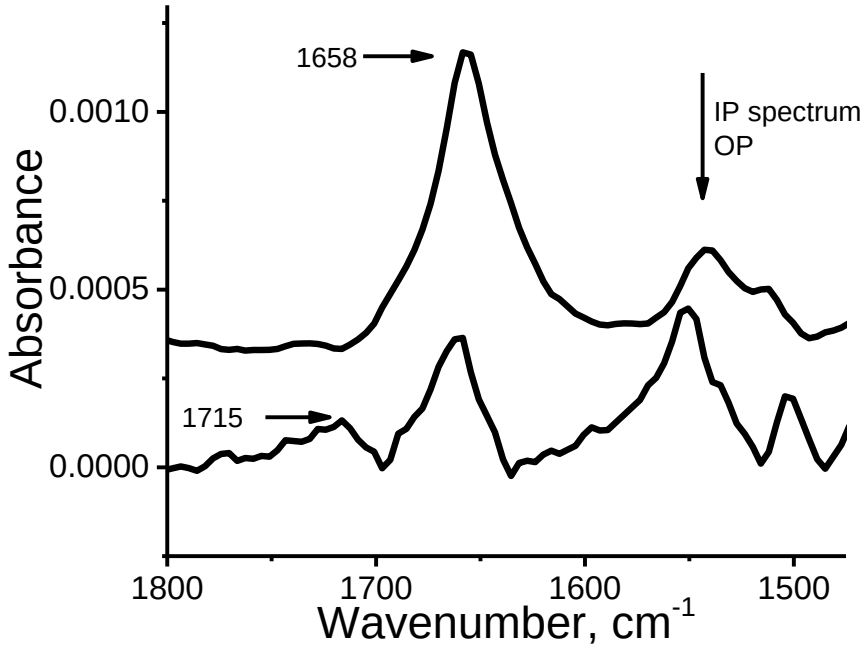

Figure 1-9. pMAIRS results of the LB monolayer of unlabeled α-syn(61－95) transferred after the surface pressure was held at 6 mN/m for two hours.

As shown in Figure 1-9 above, a peak at 1715 cm^{-1} was not detected in the IP result (the top curve in Figure 1-9) whereas detected in the OP result (the bottom curve in Figure 1-9). More interestingly, the peak at 1715 cm^{-1} was not detected in either the IP or the OP result for the monolayer of α-syn(61－95) transferred after 15 minutes compression as shown in Figure 1-5.[29] This peak indicates a probable subtle conformation change in some specific residues. To verify this hypothesis, ^{13}C label was introduced into the backbone carbonyl at position 68G and the ^{13}C labeled α-syn(61－95) will be spread at the interface.

The pMAIRS results of the monolayer of ^{13}C labeled α-syn(61－95) at 68G transferred after compression for 15 minutes are shown in Figure 1-10 below. In the IP result, which is the top curve in Figure 1-10, regular amide I and amide II bands were detected at 1658 cm^{-1} and 1555 cm^{-1}, respectively. Although containing the ^{13}C label in the backbone, the ^{13}C labeled α-syn(61－95) does not show the ^{13}C amide I band around 1625 cm^{-1} clearly in the IP result as shown before.[29] A minor shoulder was detected at approximately 1625 cm^{-1}. This is expected since the ^{13}C amide I band is not strong enough to be seen when compared to the regular amid I band at 1658 cm^{-1}, which is the sum signal of the 34 other residues, when only one ^{13}C label is present. The regular amide I band splits at 1659 and 1645 cm^{-1} in the OP result (bottom curve of Figure 1-10), which is consistent with previous publications for the unlabeled results.[29] The ^{13}C amide I band at 1625 cm^{-1} was detected in the OP result in Figure 1-10. Although suggesting a tilted (more perpendicular) orientation, the ^{13}C amide I band in the OP result overlaps with the regular amide I band (detected at 1658 and 1645 cm^{-1}), which are similar to the result as previously published.[29] The overlapping peaks make it impossible to quantitatively calculate the tilted angle of the ^{13}C amide I transition moment by Equation 1 shown in the **Introduction**. Because Figure 1-10 is the result of ^{13}C labeled α-syn(61－95) monolayer after compression for 15 minutes, the peak at 1715 cm^{-1} showing up in Figure 1-9 (i.e., the pMAIRS result of unlabeled α-syn(61－95) monolayer transferred after compression for two hours) was not detected. As published before, the ^{13}C amide I band is about 15~30 cm^{-1} lower than its regular amide I band.[29] For example, the ^{13}C amide I band of α-helix was detected at 1625 cm^{-1} (*c.f.*, the OP curve in Figure 1-10) which is also ~30 cm^{-1} lower than the regular amide I band at 1658 cm^{-1} as shown in Figure 1-10.[29] Therefore, if there is any ^{13}C amide I band derives from the regular amide I band at 1715 cm^{-1}

showing up in Figure 1-10, the position should be around 1685 cm^{-1}. But this peak was not detected in Figure 1-10, either. Consequently, we compressed the monolayer of ^{13}C labeled α-syn(61－95) for two hours and then transferred the monolayer to the substrate, which was examined by pMAIRS, and results are shown in Figure 1-11.

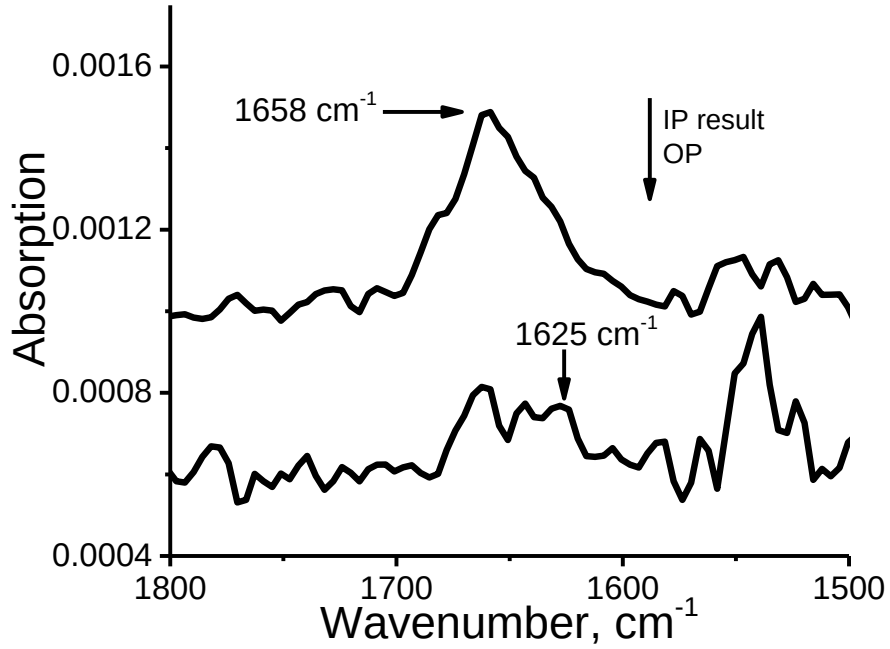

Figure 1-10. p-MAIRS results of the LB monolayer of ^{13}C labeled α-syn(61－95) at 68G transferred after the surface pressure was held at 6 mN/m for 15 minutes.

The pMAIRS results from the monolayer of ^{13}C labeled α-syn(61－95) at 68G transferred after compression for two hours are shown in Figure 1-11 compared to Figure 1-10. The IP result is similar, primarily detecting the regular amide I band at 1658 cm^{-1}. Interestingly, the OP result (bottom curve in figure 1-11) showed the presence of a novel peak at 1685 cm^{-1} in

addition to the regular and ^{13}C amide I band at 1658 and 1625 cm^{-1}, respectively. Additionally, the OP result of Figure 1-11 displays the novel peak at 1715 cm^{-1} that was found in the OP result of Figure1-9. Notice that both Figure 1-9 and 1-11 are the pMAIRS results of the monolayer of α-syn(61－95) prepared under the same condition (i.e., transferred after compression of two hours). The only difference between Figure 1-9 and Figure 1-11 is that Figure 1-11 shows the results of α-syn(61－95) with the single ^{13}C label at position 68G. Therefore, the peak at 1685 cm^{-1} in Figure 1-11 is the ^{13}C amide I band from the regular amide I band at 1715 cm^{-1}. The novel peak at 1685 cm^{-1} is clear evidence that there is subtle conformation change, specifically at 68G. Moreover, the peak at 1625 cm^{-1} was also detected as the ^{13}C amide I band of α-helix. Consequently, conformation change during the transition stage was detected.

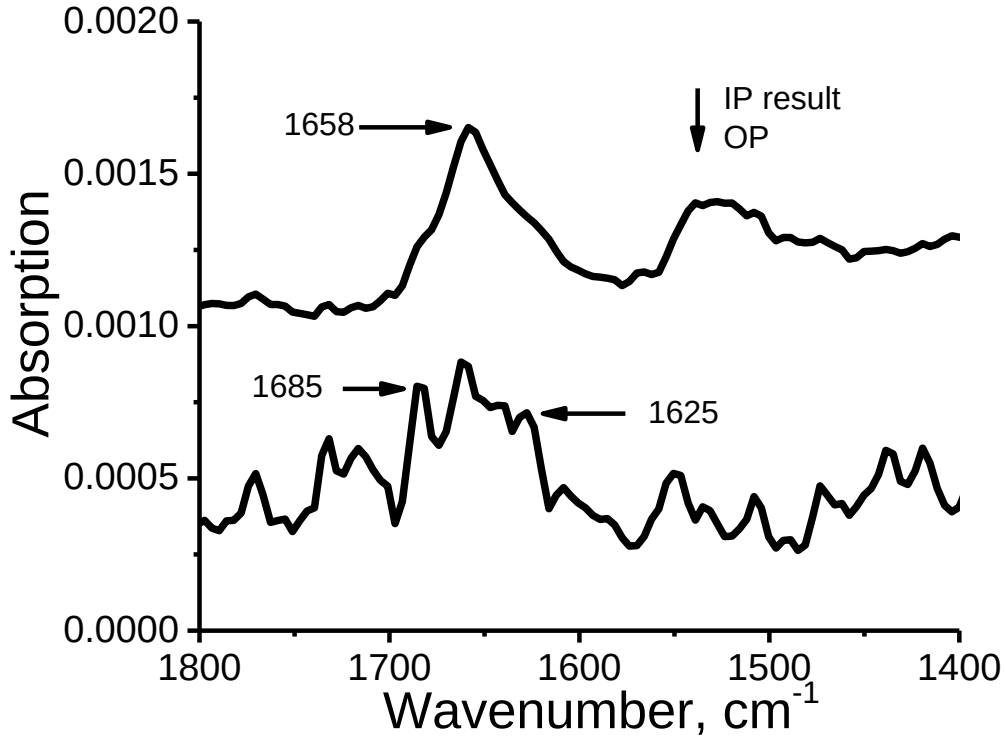

Figure 1-11. p-MAIRS results of the LB monolayer of ^{13}C labeled α-syn(61－95) at 68G transferred after the surface pressure was held at 6 mN/m for 2 hours.

It has been reported that the length of the secondary structure can also affect the amide I band position. For example, the long α-helix usually shows its amide I band around 1650 cm^{-1} whereas the short α-helix may show it around 1658 cm^{-1}.[38, 39] Because α-syn(61－95) only contains 35 residues, it is not a surprise that 1658 cm^{-1} was detected in Figures 1-9, 1-10, and 1-11. On the other hand, it has been widely accepted that anti-parallel β-sheet conformation shows its characteristic amide I bands at 1630 and 1695 cm^{-1}.[40] Although how the length affects the position of the amide I band of anti-parallel β-sheet conformation is still not very clear, we cannot rule out the probability that the peak at 1715 cm^{-1} stems from anti-parallel β-sheet conformation due to the short length of the peptide. To get more clear evidence of the formation of β-sheet conformation, the ^{13}C labeled α-syn(61－95) at 68G was compressed for three days, as shown below.

Similar to Figure 1-9 and 1-11, the regular amide I band of α-helix was detected at 1658 cm^{-1} in the S_{IP} in Figure 1-12. A shoulder peak at 1632 cm^{-1} was also detected in the $S_{IP,}$ and this peak can be assigned to the regular β-sheet conformation. In addition, no ^{13}C amide I band was clearly detected in the S_{IP} in Figure 1-12 due to the low abundance of ^{13}C label, because only one backbone carbonyl at 68G was ^{13}C labeled. As for S_{OP}, the shoulder peak at 1632 cm^{-1} was also detected, and the peak at 1685 cm^{-1} was also detected. Most importantly, the ^{13}C amide I band was detected at 1616 cm^{-1}, which is 16 cm^{-1} lower than that of the regular amide I band. Therefore, the peak at 1616 cm^{-1} is the ^{13}C amide I band of β-sheet conformation. Because only

the backbone carbonyl at 68G was ^{13}C labeled, 68G changes its conformation from helix to β-sheet after three days of compression.

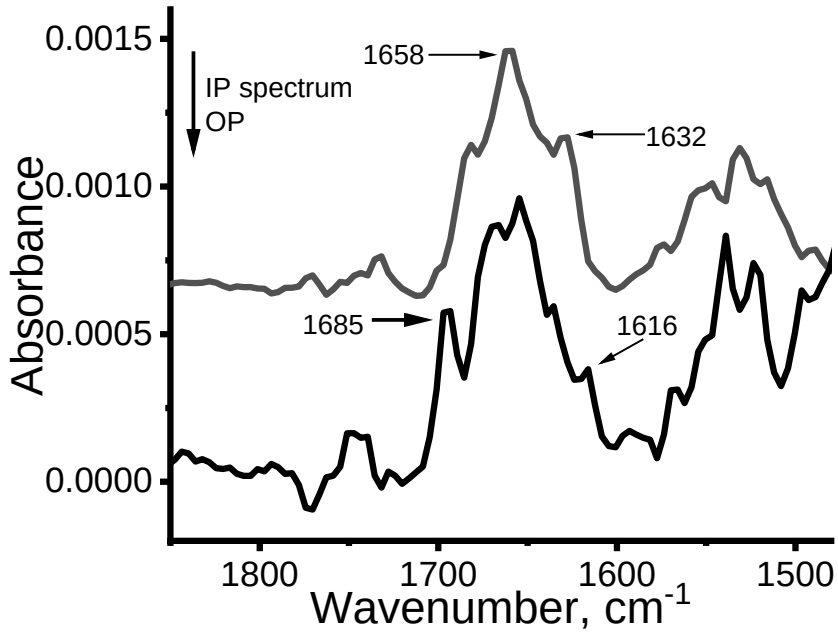

Figure 1-12. p-MAIRS results of the LB monolayer of ^{13}C labeled α-syn(61－95) at 68G transferred after the surface pressure was held at 6 mN/m for 3 days.

1.8 Conclusion of Previous Results and Thesis Motivation.

On the whole, a novel conformation was detected by pMAIRS in the monolayer of unlabeled α-syn(61－95) due to the generation of a new peak at 1715 cm^{-1} which only appears in the OP result after compression at two hours. A single ^{13}C isotope label was introduced into the backbone carbonyl of α-syn(61－95) at 68G, and the monolayer of the ^{13}C labeled α-syn(61－

95) was also analyzed by pMAIRS. After 15 minutes compression, the ^{13}C label only showed up the ^{13}C amide I band at 1625 cm^{-1} (assigned to α-helix) in the OP result. On the other hand, two ^{13}C amide I band at 1685 cm^{-1} and 1625 cm^{-1} were detected simultaneously in the OP result of pMAIRS after compression for two hours. The peak at 1685 cm^{-1}, which is 15~30 cm^{-1} lower than that at 1715 cm^{-1} was assigned to another conformation. Therefore, coexisting conformation (i.e., the transition stage during the conformation change) at specific 68G residue was detected by pMAIRS even in monolayer. After three days compression, the ^{13}C amide I band in the pMAIRS result of ^{13}C labeled α-syn(61－95) at 68G moved to 1616 cm^{-1}, which is assigned to β-sheet conformation. This suggests that the axis of α-helix at 68G or even the N-terminus is tilted to the interface as shown in Figure 1-12 below before the compression. The tilted orientation of N-terminus may facilitate the conformation change, which may result in the formation of intermolecular hydrogen bond in the N-terminus and decrease the molecular area with compression as shown in Figure 1-8. Thus, the more tilted orientation of N-terminus of α-syn(61－95) facilitates the conformation change, whereas the parallel C-terminus remains in α-helix as shown in Figure 1-12 after compression.

Then, several important questions arise. First, the N-terminus has a conformation change, as summarized in Figure 1-12. How about C-terminus after days of compression? Second, is there a difference in the speed of aggregation even between N-terminus residues? For example, will 63V aggregate to β-sheet faster than 68G? To address the questions above, ^{13}C label was also introduced into the backbone carbonyls of α-syn(61－95) at 63V. Then, the monolayer of ^{13}C labeled α-syn(61－95) at 63V or 93G was also compressed for days. pMAIRS was also used to detect conformation change in 63V and 93G. 63V was found to finish the conformation change

after 1 day compression, whereas no conformation change was detected in 93G even after 3 days compression. Detailed results are shown in Chapter 3.

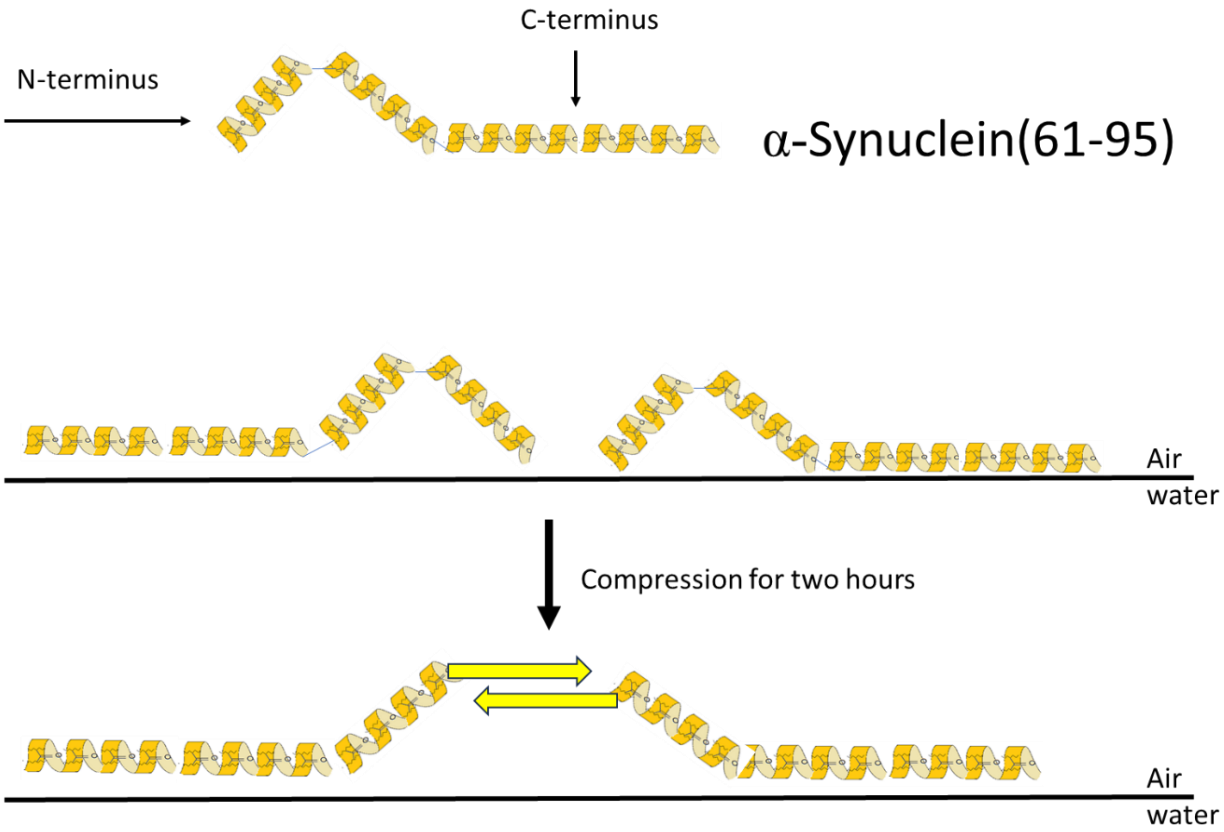

Figure 1-13. Conformation change with intermolecular hydrogen bond formation during the compression of α-syn(61－95) at the interface.

CHAPTER 2

METHODS

2.1 Materials.

Table 2.1 Listing of chemicals with purity and their respective suppliers.

The materials and their percentage purity are listed. The names of each vendor are also attached to the list below.

Materials	% Purity	Vendors
Acetonitrile	99.90	Fisher Scientific (Fairlawn, NJ)
Dichloromethane (DCM)	99.60	Fisher Scientific (Fairlawn, NJ)
Diethyl ether	99.90	Fisher Scientific (Fairlawn, NJ)
Diisopropylcarbodiimide (DIC)	99.00	Anaspec Inc. (Fremont, CA)
Fmoc-Asparagine	99.69	Chem-Impex Int'l (Wood Dale IL)
Fmoc-Alanine	99.91	Chem-Impex Int'l (Wood Dale IL)
Fmoc-Glutamine	99.61	Chem-Impex Int'l (Wood Dale IL)
Fmoc-Glutamic acid	99.11	Chem-Impex Int'l (Wood Dale IL)
Fmoc-Glycine	99.37	Chem-Impex Int'l (Wood Dale IL)
Fmoc-Isoleucine	> 98.00	Novabiochem (Hohenbrunn, Germany)
Fmoc-Leucine	99.80	Chem-Impex Int'l (Wood Dale IL)

Fmoc-Lysine	99.84	Chem-Impex Int'l (Wood Dale IL)
Fmoc-Serine	99.84	Chem-Impex Int'l (Wood Dale IL)
Fmoc-Threonine	99.60	Novabiochem (Hohenbrunn, Germany)
Fmoc-Valine	99.53	Novabiochem (Hohenbrunn, Germany)
Hydroxybenzoyltriazole (HOBT)	> 99.00	Anaspec Inc. (Fremont, CA)
Nitrogen gas	99.99	NexAir (Memphis, TN)
N,N-dimethylformamide (DMF)	99.80	Fisher Scientific (Fairlawn, NJ)
Piperidine	99.00	Sigma-Aldrich (St. Louis MO)
Silicon wafer		University Wafer Inc. (Boston MA)
Silver nitrate	99.9	Alfa Aesar (Ward Hill, MA)
Trifluoroacetic acid (TFA)	99.00	Alfa Aesar (Ward Hill, MA)
Triisopropysilane (TIS)	98.00	Sigma-Aldrich (St. Louis, MO)
Wang Resin	> 99.00	Novabiochem (Hohenbrunn, Germany)
4-dimethylaminopyridine (DMAP)	≥ 99.00	Fisher Scientific (Fairlawn, NJ)

2.2 Peptide Synthesis.

The peptides investigated in this thesis were synthesized in the laboratory using Solid Phase Peptide Synthesis (SPPS) utilizing a CEM synthesizer, as shown in Figure 2.1. In SPPS, peptides are grown from the C-terminus to the N-terminus by synthesizing the target peptide on an insoluble solid support polymer.

Figure 2.1. CEM Microwave Peptide Synthesizer.

Wang resin serves as strong support in this case because it has good swelling, mechanical strength, and stability, as shown in Figure 2.2. The resin can be cleaved efficiently in moderately acidic conditions, and side chain protecting groups can be deprotected. The amine group of individual amino acids is protected by fluorenylmethyloxycarbonylchloride (Fmoc) chemistry. Fmoc group is used to protect the amine group of each amino acid to prevent solution coupling of dissolved amino acids, and the side chains of amino acids are protected with base-stable protecting groups such as tert-butyloxycarbonyl (Boc) and t-butyl (tBu).

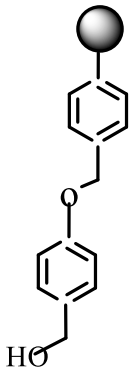

Figure 2 .2. Chemical Structure of Wang Resin.

SPPS involves the iterative steps of coupling-washing-deprotection-washing, as seen in Figure 2.3. By initiating the activation of the amino acid carboxyl catalytically with DMAP and attaching 0.2 molar equivalents of Wang resin, the C-terminal of the first Fmoc-protected amino acid was attached to Wang resin (solid support). To increase the carboxylate and reduce racemization, DIC and HOBt were introduced. An Amide bond was created when the activated carboxylate reacted with the solid support amine group. The surface of the solid phase and the resin were washed three times with DMF.

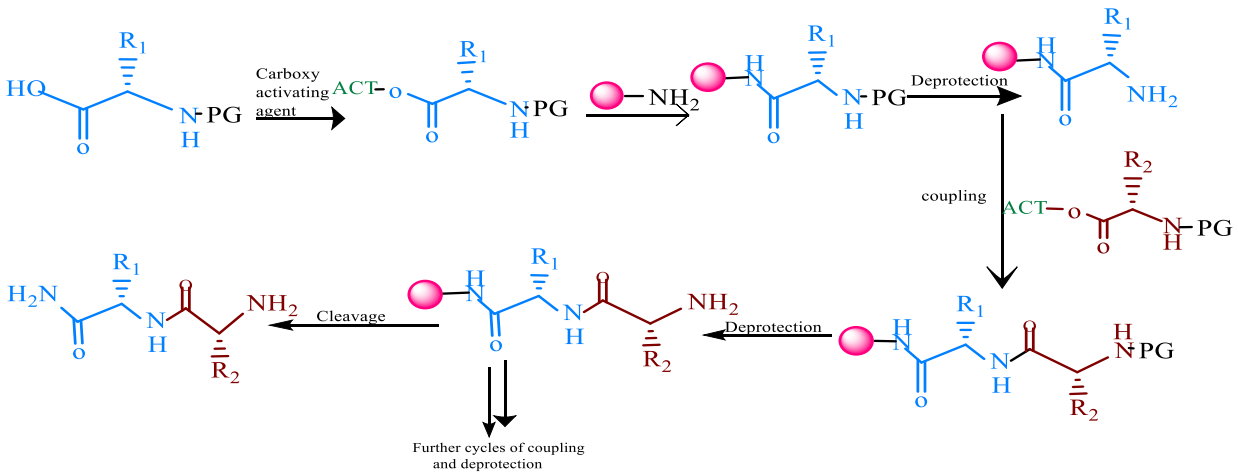

Figure. 2.3. Chemical Reaction of the General Scheme of SPPS.

The amine group is deprotected using a 1:4 (v/v) piperidine/DMF ratio to remove Fmoc. This exposes the amino acid, making it available for coupling with the next amino acids. The next step is to finish the procedure by frequently washing with DMF. The initial amino acid is linked to the solid support after the preparation and addition of the subsequent amino acid to the developing chain. The coupling–washing–deprotection–washing procedure was repeated until all the necessary amino acids were coupled. The peptide was cleaved from the resin once the desired sequence was obtained. Figure 2.4 shows how the peptide was suspended in a solution containing 75% TFA, 22% DCM, 1.5% TIS, and 1.5% H_2O and shaken periodically to break the bond between the resin and the peptide's C-terminal carboxylic group. At the side chain deprotection stage, adding H_2O and TIS prevents side reactions, while TFA deprotects side chains by removing protective groups like Boc and tBu. DCM, TIS, TFA, and H_2O were

removed by purging with nitrogen. The peptide was centrifuged, and the liquid was decanted after diethyl ether was added, leaving the crude synthetic peptide product behind.

Figure 2.4: Cleavage Process using TFA.

2.3 Conditions for Mass Spectrometer.

The successful synthesis of the peptide was confirmed using a compact QTOF mass spectrometer (equipped with Compass 1.9 and QTOF Control 4.0 software) linked to electrospray ionization (ESI) Apollo source (Bruker Daltonic GmbH & Co. KG). Using a solvent mixture of 50% acetonitrile (ACN) and 0.1% formic acid (FA) as the mobile phase, the synthesized peptide was injected into a chromatography column. At a spectral acquisition rate of 4 Hz, the analysis was carried out in positive-ion mode. A drying temperature of 180°C was maintained by providing nitrogen gas at a pressure of 0.6 bar. 7.0 eV was chosen as the collision

energy. Within the mass-to-charge ratio (m/z) range of 100, data for each collision energy were gathered over a 3-minute period.

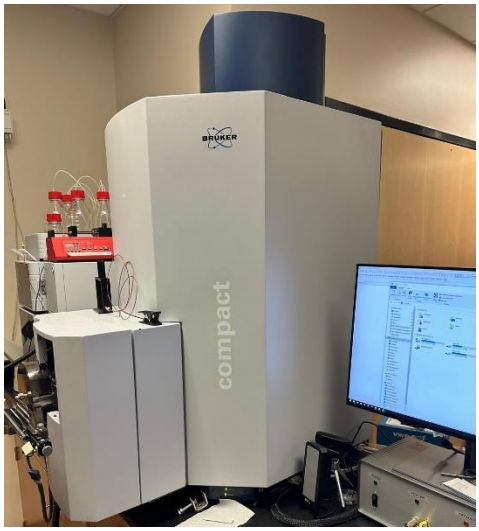

Figure 2.5. Compact QTOF interfaced with an electrospray ionization (ESI)

2.4 Conditions for High-Performance Liquid Chromatography.

High-performance liquid chromatography (HPLC) was used to purify every protein produced for this thesis. A chromatographic column filled with porous materials is used by the HPLC apparatus, and substances are separated according to how well they bind to the surface of the porous materials. **Figure 2.5** shows a Phenomenex Reverse Phase Semi Prep C18 Column, Jupiter Model 00G-4055-P0, with column dimensions of internal diameter of 21.5 mm and length of 250 mm (Phenomenex, Inc. Torrence, CA), attached to a Waters 1525 Binary Solvent Pump (Waters Corp., Milford, MA) where protein purification was carried out. A 250 nm UV

absorption wavelength was used for the detection using a Waters 2489 UV-Vis detector (Waters Corp., Milford, MA). Ultra-pure water and 0.1% TFA (v/v) were the ingredients of mobile phase A, while HPLC-grade acetonitrile and 0.1% TFA (v/v) made up mobile phase B. A linear gradient of 8 to 16 percent by volume of A and 92% to 84% by volume of B was used for the separation process, which lasted 50 minutes at a flow rate of 21.5 mL/minute. The purification procedure was applied to the crude products after validating the target peptide's molecular weight and determining its retention time using the Mass Spectrometer. The purified fractions were then collected, refrigerated at -80 °C, and lyophilized to get the pure solid peptide.

Figure 2.6. Waters 1525 System High Performance Liquid Chromatograph

2.5 Conditions for Langmuir Monolayer Trough.

The stability of the surface pressure-area (π-A) isotherm of the Langmuir monolayer of α-syn (61-95) on pure water subphase and the deposition of its LB film to silica slides were examined using the Kibron μtrough Langmuir trough XS (Kibron Inc., Helsinki, Finland), as illustrated in **Figure 2.7**. The α-syn (61-95) aqueous solution had a 1.5 mg/mL concentration. A 25 μL syringe (Hamilton Inc., Reno, Nevada) held less than 1 cm from the subphase surface was used for spreading the α-syn (61-95) at the air-water interface, and the monolayer formation process took 30 minutes. To make the Langmuir-Blodgett films of α-Syn (61-95), the α-syn (61-95) Langmuir monolayer was transferred to the silicon wafer at a surface pressure of 6 mN/m. After being held at different points before transference, the silicon wafer was moved gently at a speed of 0.3 cm/minute.

Figure 2.7. Kibron Langmuir Trough

2.6 p-Polarized Multiple-Angle Incidence Resolution Spectroscopy (pMAIRS).

pMAIRS was carried out by placing the LB film monolayer on the silicon (Si) substrate in the pMAIRS accessory and passing an IR beam through the sample using a Thermo Fisher

Scientific Nicolet iS50R FT-IR spectrometer fitted with a pMAIRS accessory, as seen in **Figure 2.8**. The refractive IR beam was directed toward the HgCdTe (MCT A) detector. The α-syn(61－95) spectra were acquired using a 50 kHz modulation on a bare Si substrate as the background. The background and sample spectra were collected across nine thousand scans at a resolution of 8 cm^{-1}. The in-plane (IP) and out-of-plane (OP) spectra were estimated using background and sample data at incident angles ranging from 9 º to 44 º. To find the orientation angle of the amide I band to the surface normal (i.e., in Equation 1), the following equation was used:

$$\phi = \tan^{-1}\sqrt{\frac{2A_{IP}}{A_{OP}}}$$

Where A_{IP} represents the peak area of the amide, 1 band in the IP spectrum, while A_{OP} is that of the amide I band in the OP spectrum. The tilt angle of the amide I transition moments with the surface equals 90 º minus ϕ (i.e., 90 º - ϕ).

2.8. Thermo Fisher Nicolet iS50R FTIR with electronic rotary stage component

CHAPTER 3

RESULTS AND DISCUSSION

3.1 Validation of Success of Synthesis and Purification for α-Syn(61－95) by QTOF-MS.

In our previous reports, the Waters Q-Tof was shown to not work on our sample. Bruker Q-Tof Mass spectrometer was then used to confirm the success of the synthesis of unlabeled α-syn(61－95). Here, we continued to utilize the Bruker Q-Tof to confirm that the ^{13}C label was indeed introduced into the correct position. Figure 3-1 shows the fragmental MS/MS result of ^{13}C labeled α-syn(61－95) at the backbone carbonyl (i.e., C=O) of 68G position. The dominant peaks were detected around 1652.5017 Da, which is the parent ions of ^{13}C labeled α-syn(61－95) with two positive charges as reported before. It is worth noting that the fragment MS/MS results of ^{13}C labeled α-syn(61－95) at 63V and 93G are identical to that of 68G, as shown in Figure 3-1. This is because the overall molecular weight of the three peptides are the same at 3303 Da, and the only difference between them should stem from the fragments due to the difference in labeled position. To confirm this, the low mass result and high mass result of fragment MS/MS are shown in Figure 3-2 and 3-3, respectively.

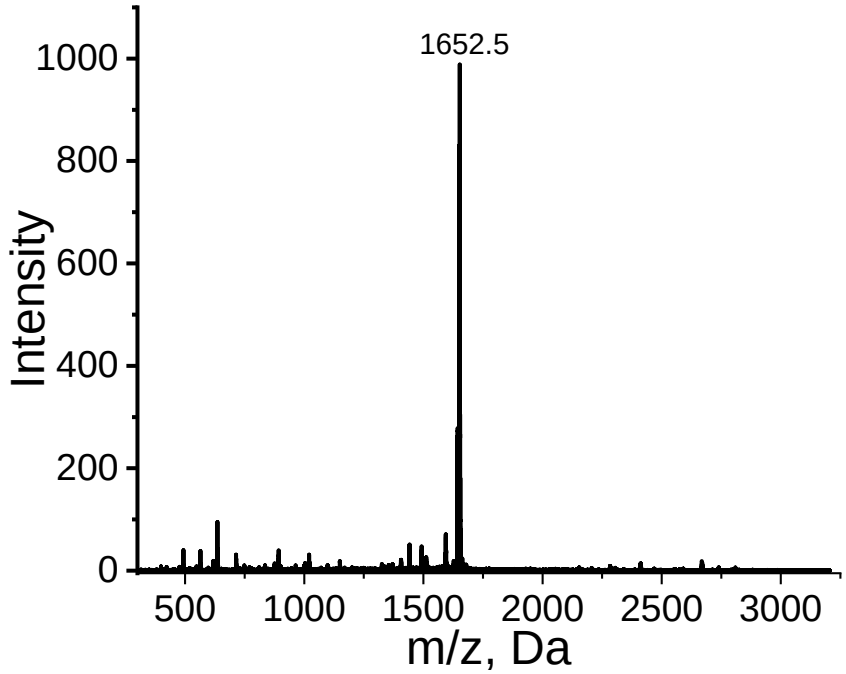

Figure 3-1. Overall fragment MS/MS spectroscopy of ^{13}C labeled α-syn(61－95) at the backbone carbonyl of 68G.

As shown in the Figure 3-2 which covers the low mass fragment MS/MS result from Figure 3-1 from 300~ 1600 Da, about 65% of the peaks can be assigned. However, about 20% peak with high signal-to-noise ratio cannot be assigned well. For example, the peaks at 1511.8316, 1097.6359 713.4169, and 618.3345 Da are with excellent signal-to-noise ratios but cannot be assigned to any probable fragment of α-syn(61－95). If these peaks are not reliable, the reliability of other peaks is negatively affected even if they can be assigned well. We will continue to learn to improve the data quality of low mass fragment MS/MS.

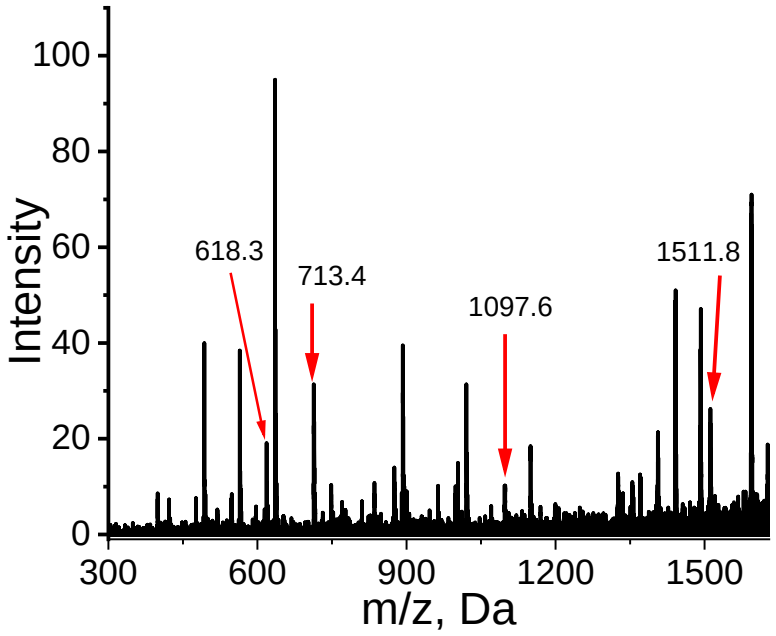

Figure 3-2. Low Mass fragments MS/MS spectroscopy of ^{13}C labeled α-syn(61－95) at the backbone carbonyl of 68G.

On the contrary, all the peaks with good signal-to-noise ratio in the high mass part of the fragment MS/MS spectroscopy of ^{13}C labeled α-syn(61－95) at 68G can be assigned well, as shown in Figure 3-3 below. For example, the peaks at 2811.6355, 2740.5438, and 2669.6854 Da can be assigned to fragments of α-syn(61－95) with sequences of 61~90, 61~89, and 61~88, respectively. The peaks at 2413.4075, 2284.2459, and 2155.3139 Da can be assigned to the fragments with sequence of 61~85, 61~83, and 61~82, respectively. The fragments with sequence of 61~87, 61~86, and 61~84 were also detected as marked by an asterisk (i.e., *) in Figure 3-3. It is worth noting that the peaks marked in red are assigned to fragments with a complete N-terminus, which starts from residue 61. On the other hand, fragments from the C-

terminus ending with residue 95 were also detected and marked in green in Figure 3-3. For example, the peak at 2590.5440 Da can be assigned to fragment 67~95, and that at 2304.4044 Da is for 71~95. The peak at 2206.3191 Da is for 72~95. So far, we do not know the reason more N-terminus fragments were detected than the C-terminus ones. We plan to continue to learn and improve our skill for the Bruker Q-tof instrument. Anyway, the results shown in Figure 3-3 is enough to enable us to confirm the position of ^{13}C label is correct as described below.

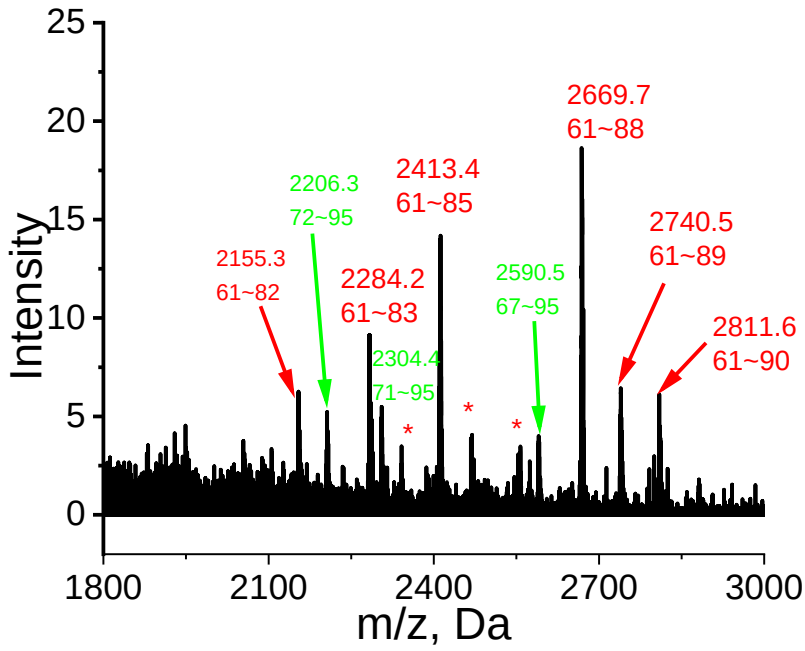

Figure 3-3. High mass fragment MS/MS spectroscopy of ^{13}C labeled α-syn(61－95) at the backbone carbonyl of 68G.

Notice that every peak marked in Figure 3-3 contains a bunch of peaks. For example, Figure 3-4 shows the enlarged figure of peaks around 2669.6854 Da in Figure 3-3 overlaid together with

also the results of the ^{13}C labeled of α-syn(61－95) at 93G and 63V. In the curve of 68G (the middle one), the peak 2669.6854 Da is the highest among the bunch of peaks, and the difference between the neighboring peaks is 1 Da, which is due to the randomly distributed isotope of ^{13}C (the major isotope because of its 1.16 % abundance), deuterium, and so on. As mentioned above, the peaks around 2669.6854 Da are assigned to the fragment with sequence of 61~88. Therefore, the most abundant peak of the fragment MS/MS spectroscopy of 93G is at 2668.7242 Da. This is because the ^{13}C label in the ^{13}C labeled α-syn(61－95) is at 93G, which is not in the fragment of 61~88. On the contrary, the ^{13}C label in α-syn(61－95) at 68G or 63V is in the fragment of 61~88. Therefore, the strongest peak in the fragment MS/MS results of 68G and 63V is at 2669.6854 Da which is 1 Da higher than that of 93G.

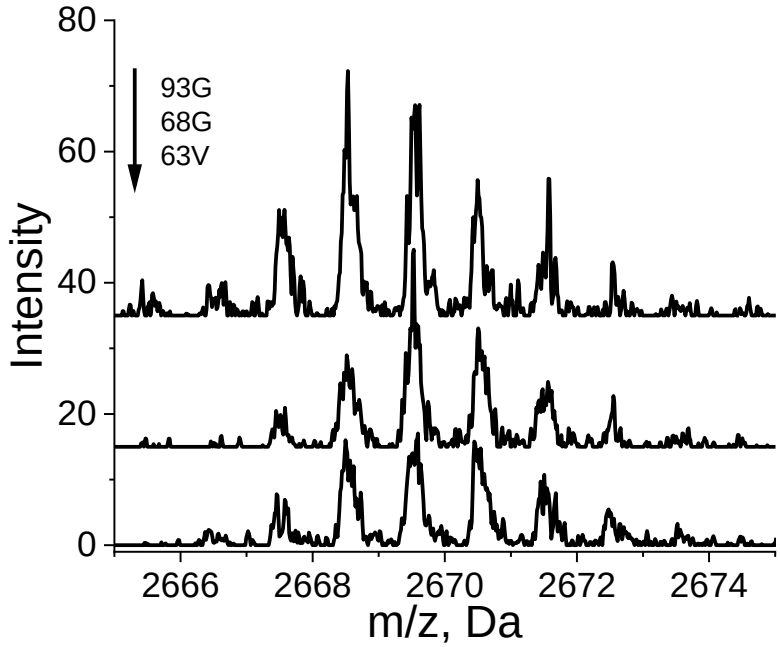

Figure 3-4. Overlaid fragment MS/MS spectroscopy of ^{13}C labeled α-syn(61－95) at the backbone carbonyl of 93G, 68G, and 63V around 2669.6854 Da.

Then, how can we confirm the position of the ^{13}C label at 68G and 63V? The peaks around 2590.5440 Da are needed because they stem from the fragment of 67~95 and the overlaid results are shown in Figure 3-5. Since the ^{13}C label in the ^{13}C labeled α-syn(61－95) at 63V is not in the fragment of 67~95, the most abundant peak of the result of 63V (the bottom curve) of Figure 3-5 is at 2589.5438 Da. On the contrary, the results of both 68G and 93G show the strongest peak at 2590.5440 Da, because both of them contain the ^{13}C label in the fragment of 67~95. Due to the reasonable outcomes in the results above, the position of ^{13}C label is confirmed. We will continue to learn how to use the Bruker Q-TOF spectrometer and optimize the fragment MS/MS results.

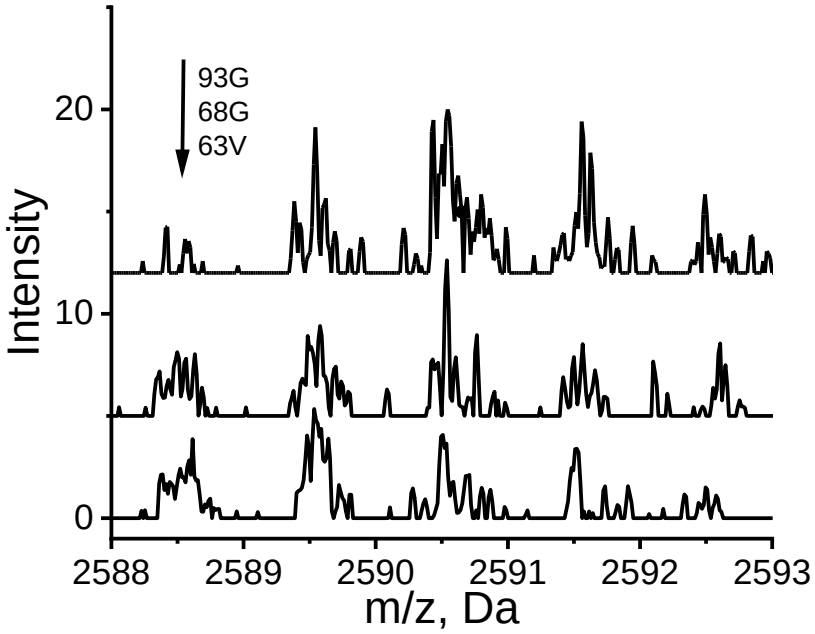

Figure 3-5. Overlaid fragment MS/MS spectroscopy of ^{13}C labeled α-syn(61－95) at the backbone carbonyl of 93G, 68G, and 63V around 2590.5440 Da.

3.2 Conformation Change in Specific Residues were Detected by pMAIRS

After the confirmation of the success in ^{13}C labeling in the sequence of α-syn(61－95), we paid our attention back to the conformation study of α-syn(61－95) by pMAIRS. Figure 3-6 below shows the pMAIRS results of the monolayer of unlabeled α-syn(61－95) transferred onto Si substrate after three days compression at 6 mN/m. Compared with short time compression results shown in Figure 1-5 in Chapter One, there is no big change in the S_{IP} and the major peak is still at 1658 cm^{-1}, which is the typical position for α-helix. On the other hand, the typical peak position for β-sheet at 1633 cm^{-1} was clearly detected in the S_{OP}. Therefore, Figure 3-6 clearly shows that substantial residues in the sequence of α-syn(61－95) has changed their conformation from α-helix to β-sheet. Now the question is: where does the conformation change occur? In C-terminus residues or N-terminus residues? To address this question, the pMAIRS were used to study the ^{13}C labeled α-syn(61－95) at 93G, 68G, and 63V after long time compression.

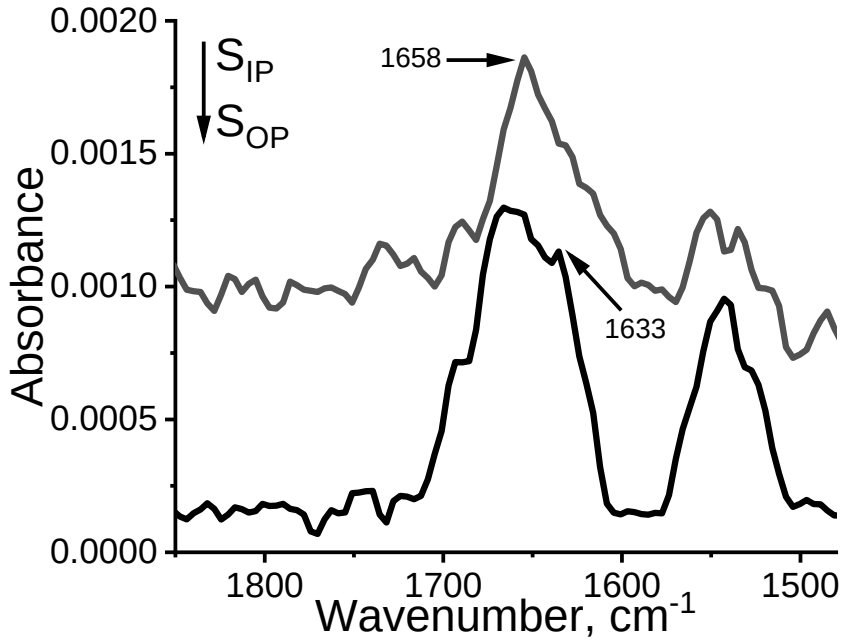

Figure 3-6. p-MAIRS results of the LB monolayer of unlabeled α-syn(61－95) transferred after the surface pressure was held at 6 mN/m for three days.

Figure 3-7 below shows the pMAIRS results of the monolayer of ^{13}C labeled α-syn(61－95) at 93G after three days of compression at 6 mN/m. The S_{IP} curve (the top one) is very similar to the results of short time compression for ^{13}C labeled α-syn(61－95) at 93G shown in Figure 1-7. The peak at 1658 cm^{-1} together with the ^{13}C amide I band of helix at 1625 cm^{-1} (also shown in Figure 1-7), was detected in the S_{IP} in Figure 3-7. Interestingly, the ^{13}C amide I band of helix at 1625 cm^{-1} is also detected in the S_{OP} curve as a shoulder peak at the bottom of Figure 3-7. This is different from the S_{OP} in Figure 1-7 and indicates that the orientation of helix at 93G became a little more tilted than short term compression compared with those shown in Figure 1-7. On the

whole, 93G is still in helical conformation after three days of compression. On the contrary, obvious change in the peak position was detected in the pMAIRS results of the monolayer of ^{13}C labeled α-syn(61－95) at 68G compressed for three days. The results below show the dynamic change under compression with increasing time.

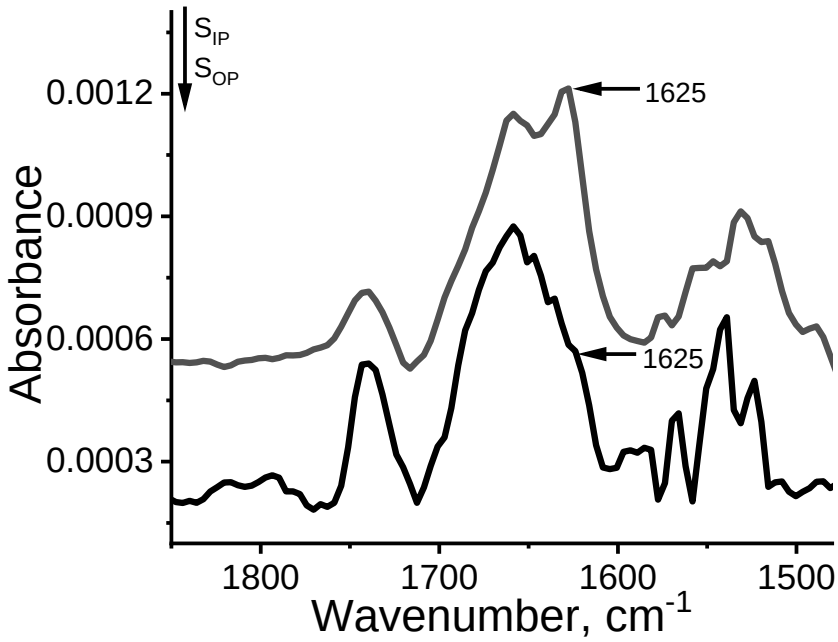

Figure 3-7. p-MAIRS results of the LB monolayer of ^{13}C labeled α-syn(61－95) at 93G transferred after the surface pressure was held at 6 mN/m for three days.

The pMAIRS results of the monolayer of ^{13}C labeled α-syn(61－95) at 68G with one day compression is shown in Figure 3-8. Overall, Figure 3-8 is similar to the results with two hours compression as shown in Figure 1-10. For example, the major peak detected in S_{IP} is 1658 cm^{-1}.

In S_{OP}, shoulder peaks were detected in 1625, 1685, and 1717 cm^{-1}. This indicates that residue 68G is still in α-helix. However, it was shown in Figure 1-12 that 68G changes to β-sheet after three days compression. When compared with Figures 1-12 and 3-8, we can find that the major change was detected in the S_{OP} results. Therefore, S_{OP} results overlays in Figure 3-9 and the gradual conformation change is detected when the compression time increases. As for the one-day result, the shoulder peak was detected in 1625 cm^{-1}, and this peak became broader in two days result. When compression reached three days, the shoulder peak at 1625 cm^{-1} completely disappeared and a novel peak at 1616 cm^{-1} generated. Therefore, the broader and weaker shoulder peak around 1620 cm^{-1} shows the coexistence of α-helix and β-sheet for residue 68G. In other words, the transition during the conformation change at 68G was snapshot by pMAIRS.

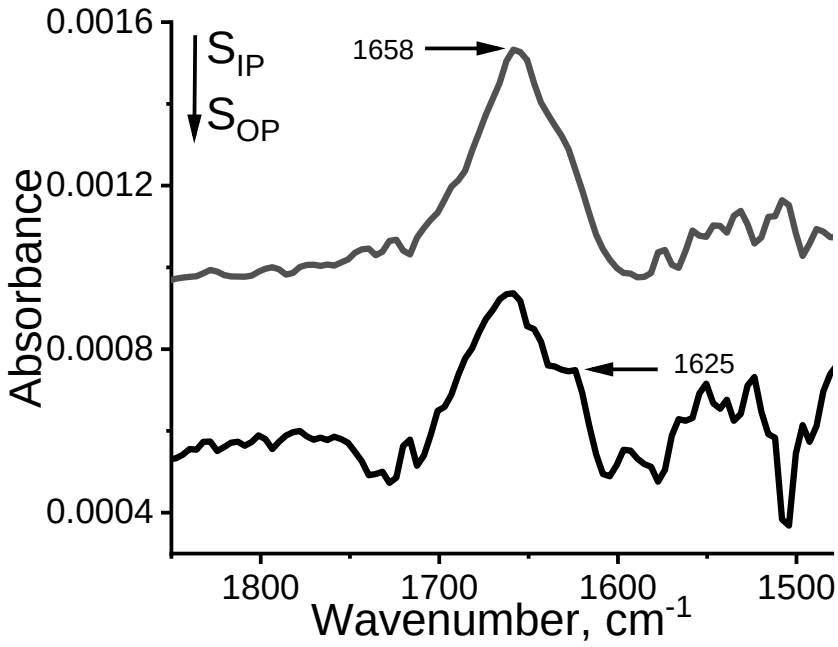

Figure 3-8. p-MAIRS results of the LB monolayer of ^{13}C labeled α-syn(61－95) at 68G transferred after the surface pressure was held at 6 mN/m for one day.

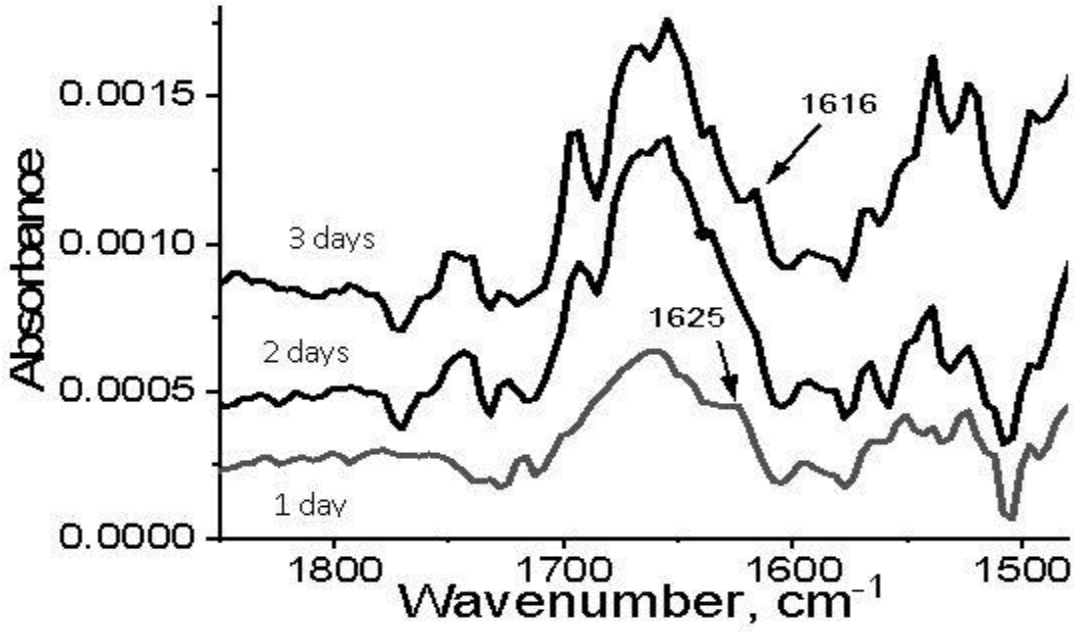

Figure 3-9. S_{OP} results of the LB monolayer of ^{13}C labeled α-syn(61－95) at 68G transferred after the surface pressure was held at one, two, and three days.

Similarly to 68G, residue 63V was found to also change its conformation from α-helix to β-sheet during the compression. However, 63V changes its conformation only in two days which is faster than 68G. Figure 3-10 shows the pMAIRS results of ^{13}C labeled α-syn(61－95) at 63V after two days compression. In the S_{IP} (the top curve) of Figure 3-10, peaks of 1658 and 1632 cm^{-1} were detected. As mentioned above, 1658 cm^{-1} is typical position for α-helix and 1632 cm^{-1} was for β-sheet. Interestingly, the shoulder peak at 1616 cm^{-1} was detected in the S_{OP} of Figure 3-

10. This peak is the ^{13}C amide I band for β-sheet as discussed before. Overall, Figure 3-10 is similar to Figure 1-12 and shows that 63V changes its conformation from α-helix to β-sheet faster (only two days) than 68G.

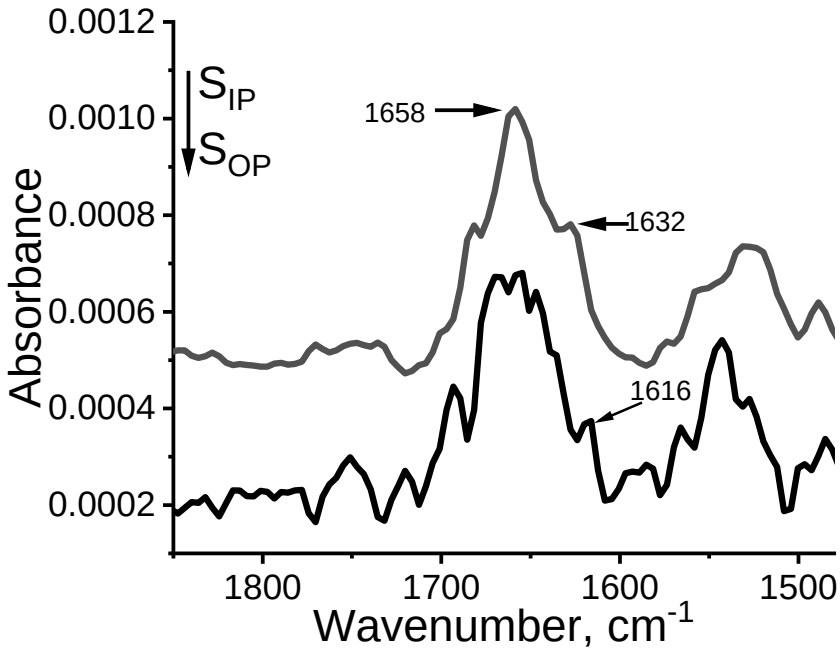

Figure 3-10. p-MAIRS results of the LB monolayer of ^{13}C labeled α-syn(61－95) at 63V transferred after the surface pressure was held at 6 mN/m for two days.

3.3 Discussion and Conclusion

Overall, conformation change from α-helix to β-sheet was detected in N-terminus residues in α-syn(61－95). Furthermore, residues closer to N-terminus may show a faster rate for the conformation change because 63V changes its conformation faster than 68G. Interestingly, the

S_{OP} in pMAIRS results is more sensitive than S_{IP} to detect β-sheet. For example, a novel peak at 1717 cm^{-1} was detected in the S_{OP} in Figure 1-9 for unlabeled α-syn(61－95) after two hours compression. In addition, 1685 cm^{-1} was detected for the ^{13}C labeled α-syn(61－95) either in 68G (e.g., Figure 1-11 and 3-9) or in 63V (e.g., Figure 3-10). Moreover, the peak at 1616 cm^{-1} which is the ^{13}C amide I band for β-sheet was only clearly detected in S_{OP} results such as in Figure 3-9 and 3-10. This may be due to the orientation of β-sheet conformation at the air-water interface as shown in Figure 3-11 below.

There are three probable orientations of β-sheet at the interface, namely, face-up, edge-up, and strand up as shown in Figure 3-11A, B, and C, respectively. It is worth noting that the backbone carbonyls inside the β-sheet strand is roughly perpendicular to the strand. Therefore, the backbone carbonyls in the face-up and strand-up orientation will be parallel to the interface. This parallel orientation will result in a strong signal in S_{IP} as shown in Figure 1-7. However, this is not the case as detected in the Figures in Chapter three. Therefore, the orientation of β-sheet in the N-terminus of α-syn(61－95) at interface is edge-up as shown in Figure 3-11B.

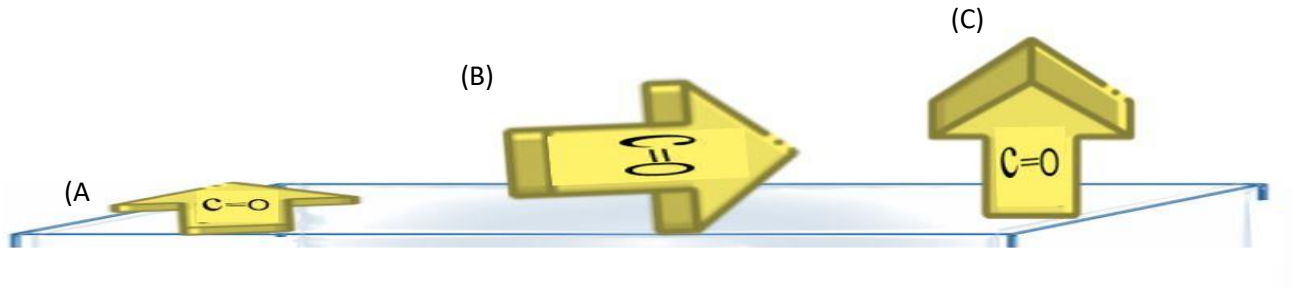

Figure 3-11. Probable orientation of α-syn(61－95) at the interface.

REFERENCES

1. M. Chen, M. Margittai, J. Chen and R. Langen, J. Biol. Chem. **282**, 24970-24979 (2007).
2. H. Heise, W. Hoyer, S. Becker, O. C. Andronesi, D. Riedel and M. Baldus, Proc. Nat. Acad. Sci. U.S.A. **102** (15871-15876) (2005).
3. W. H. Massover, J. Synchrotron Radiat. **14**, 116-127 (2007).
4. Y. Cheng, Curr. Opin. Struct. Biol. **52**, 58-63 (2018).
5. A. Krogh, B. Larsson, G. Heijne and E. L. L. Sonnhammer, J. Struct. Biol. **305**, 567-580 (2001).
6. J. Manor, E. Arbely, A. Beerlink, M. Akkawi and I. T. Arkin, J. PHys. Chem. Lett. **5**, 2573-2579 (2014).
7. X. Yao, X. Fan and N. Yan, Proc. Nat. Acad. Sci. U.S.A. **117**, 18497-18503 (2020).
8. C. G. Dudzik, E. D. Walter, B. S. Abrams, M. S. Jurica and G. L. Millhauser, Biochemistry **52**, 53-60 (2013).
9. M. G. Spillantini, R. A. Crowther, R. Jakes, M. Hasegawa and M. Goedert, Proc. Natl. Acad. Sci. U. S. A. **95**, 6469-6473 (1998).
10. M. G. Spillantini, M. L. Schmidt, V. M. Y. Lee, J. Q. Trojanowski, R. Jakes and M. Goedert, Nature **388**, 839-840 (1997).
11. K. Beyer, Acta Neuropathol. **112**, 237–251 (2006).
12. G. Yang, Y. Dong, K. Gong, W. Jiang, E. Kwon, P. Wang, H. Zheng, X. Zhang, W. Gan and N. Zhao, Neurosci. Lett. **384**, 66-71 (2005).
13. Z. Qin, D. Hu, S. Han, D. Hong and A. L. Fink, Biochemistry **46**, 13322-13330 (2007).
14. L. Breydo, J. W. Wu and V. N. Uversky, Biochim. Biophys. Acta. **1822**, 261-285 (2012).

15. H. Han, P. H. Weinreb and P. T. Lansbury, Chem. Biol. **2**, 163-169 (1995).

16. R. Kahn, P. Carpentier, C. Berthet-Colominas, M. Capitan, M. L. Chesne, E. Fanchon, S. Lequien, D. Thiaudiere, J. Z. Vicat, P. and H. Stuhrmann, J. Synchront. Rad. **7**, 131-138 (2000).

17. J. K. Lanyi, Mol. Membrane Biol. **21**, 143-150 (2004).

18. Y. Xu and S. Dang, Front. Mol. Biosci. **9**, 892459 (2022).

19. L. Zhou and D. Kurouski, Anal. Chem. **92**, 6806-6810 (2020).

20. R. M. Fabre, G. O. Okeyo and D. R. Talham, Langmuir **28**, 2835-2841 (2012).

21. R. M. Nyffenegger and R. M. Penner, Chem. Rev. **97**, 1195-1230 (1997).

22. T. Hasegawa, *Quantitative Infrared spectroscopy for understanding of a condensed matter*. (Springer 2017).

23. O. Teschke and E. F. de Souza, Langmuir **18**, 6513-6520 (2002).

24. O. Teschke and E. F. de Souza, Chem. Phys. Lett. **403**, 95-101 (2005).

25. L. Dziri, B. Desbat and R. M. Leblanc, J. Am. Chem. Soc. **121**, 9618-9625 (1999).

26. R. M. Fabre and D. R. Talham, Langmuir **25**, 12644-12652 (2009).

27. X. Du, W. Miao and Y. Liang, J. Phys. Chem. B **109**, 7428-7434 (2005).

28. T. Hasegawa, J. Nishijo, M. Watanabe, J. Umemura, Y. Ma, G. Sui, Q. Huo and R. M. Leblanc, Langmuir (12), 4758-4764 (2002).

29. C. Wang, S. K. Sharma, S. O. Olaluwoye, S. A. Alrashdi, T. Hasegawa and R. M. Leblanc, Colloid. Surf. B **183**, 110401 (2019).

30. C. Wang, Y. Zhou, C. Ewuola, T. Akinleye, T. Hasegawa and R. M. Leblanc, Anal. Sci. **38**, 935-940 (2022).

31. S. M. Decatur, Acc. Chem. Res. **39**, 169-175 (2006).

32. E. Maltseva, A. Kerth, A. Blume, H. Mohwald and G. Brezesinski, Chembiochem **6**, 1817-1824 (2005).

33. C. Wang, N. Shah, G. Thakur, F. Zhou and R. M. Leblanc, Chem. Commun. **46**, 6702-6704 (2010).

34. A. L. Fink, Acc. Chem. Res. **39**, 628-634 (2006).

35. S. A. Petty and S. M. Decatur, J. Am. Chem. Soc. **127**, 13488-13489 (2005).

36. S. Li, J. D. Combs, O. E. Alharbi, J. Kong, C. Wang and R. M. Leblanc, Chem. Commun. **51**, 12537-12539 (2015).

37. S. Li, P. Sneha, J. D. Keith, C. Wang and R. M. Leblanc, Chem. Commun. **50**, 3931-3933 (2014).

38. L. Pauling and R. B. Corey, Proc. Nat. Acad. Sci. U.S.A. **37**, 729-740 (1951).

39. E. Goormaghtigh, V. Cabiaux and J. M. Ruysschaert, Subcell. Biochem. **23**, 329-450 (1994).

40. N. Demirdoven, C. M. Cheatum, H. S. Chung, M. Khalil, J. Knoester and A. Tokmakoff, J. Am. Chem. Soc. **126**, 7981-7990 (2004).